Rigid Body Cable for Virtual Environments

Martin Servin, and Claude Lacoursière,

***Abstract*— The present paper addresses real-time simulation of cables for virtual environments. A faithful physical model based on constrained rigid bodies is introduced and discretized. The performance and stability of the numerical method are analyzed in detail and found to meet the requirements of interactive heavy hoisting simulations. The physical model is well behaved in the limit of infinite stiffness as well as in the elastic regime, and the tuning parameters correspond directly to conventional material constants. The integration scheme mixes the well known Störmer-Verlet method for the dynamics equations with the linearly implicit Euler method for the constraint equations and enables physical constraint relaxation and stabilization terms. The technique is shown to have superior numerical stability properties in comparison with either chain link systems, or spring and damper models. Experimental results are presented to show that the method results in stable, real-time simulations. Stability persists for moderately large fixed integration step of $\Delta t = 1/60$ s, with hoisting loads of up to 10^5 times heavier than the elements of the cable. Further numerical experiments validating the physical model are also presented.**

***Index Terms*— hoisting cable, interactive simulation, virtual environment, multibody system dynamics, elasticity, numerical stability, numerical integration.**

I. Introduction

Virtual environments (VE) are interactive visual simulations enabling experiences that may be difficult, costly, dangerous, or just impossible to realize in practice. VE-based systems are used extensively in commercial applications such as heavy machine operator or surgeons training systems, for instance. VEs are also used in applications ranging from robotics, early-stage virtual prototyping, and interactive entertainment, to name just a few. Fast physics integrators are also useful in molecular dynamics and other areas of basic scientific research.

Robust visual simulations of real-world phenomena at interactive rates requires both efficient numerical methods as well as expressive physical models *compatible* with each other. There is increasing demand both for increased speed, stability, and efficiency, and for increased modeling expressiveness.

Rigid multibody systems dynamics [35] is a fundamental component of physics-based VEs. Both the literature and the software offering for rigid multibody system has reached some level of maturity. There are many software packages available for simulating these systems. Techniques for more complex physical systems, such as deformable solids, fluids, and granular materials, among many others, are actively developed. There are several introductory textbooks [11] as well as monographs, research papers, and review articles available.

Manuscript submitted June 13, 2007.

M. Servin is at Department of Physics at Umeå University.

C. Lacoursière is at HPC2N/VRlab and Computing Science Department at Umeå University.

Realism in VEs depends more strongly on the *global preservation of invariants*, such as energy and momentum, for instance, than on local accuracy of trajectories. This contrasts with the canonical wisdom of numerical analysis where higher order methods are favored. Indeed, higher order methods are usually more stable and allow larger integration step, still providing very good local accuracy. They usually do less work for given accuracy and stability requirements. However, this is not necessarily true if the user inputs are unpredictable or non-smooth, since higher order methods have to be restarted at each discontinuity. If one strives for maximum stability for the minimum work per step, as well as a predictable work load, a stable one-step, one-stage, fixed time-step method [14] is the best choice. In addition, high order integration methods do not necessarily guarantee global bounds on the fluctuation of physical invariants. Unless one uses an energy preserving or a symplectic method, the value of energy could increase or decrease monotonically over time. However, variational integration methods, even the merely consistent ones such as the symplectic Euler scheme, do provide global bounds on energy fluctuation and exactly preserve a discrete momentum [18]. For a mechanical system, a global bound on energy fluctuations corresponds to a stability guarantee as well.

The focus of the present paper is the simulation of cables used in hoisting devices for VEs. These are used in simulator applications involving cranes of different types. Hoisting cables are often made of steel wires though chains are also used.

Simulation of hoisting cables in VEs is subject to a number of slightly conflicting requirements, as listed in § I-A. There is no previously existing combination of physical model and numerical method fulfilling all these requirements, motivating the new physical model and computational techniques presented herein.

A. Requirements for hoisting cable

The requirements for simulation of hoisting cables in a VE application are now listed. (i) *Real-time:* the simulation should run in real-time at a fixed rate of 60 Hz to integrate with standard VE applications; (ii) *Stability:* variations of energy should be globally bounded, and the bound should be moderately small, of the order of a few percent; (iii) *High mass ratios:* real hoisting cables can hold up loads more than 10,000 times their own weight; (iv) *Physical elasticity:* parametrization of elasticity parameters for stretching, bending and torsion should correspond directly to known physical data; (v) *High stiffness:* heavy hoisting cables are extremely stiff with respect to stretching, bending, and torsion; (vi) *Scene interaction:* the virtual cable should interact with other objects usually found in VE scenes via non-penetration constraints generating dry frictional contacts, or explicit attachments to rigid bodies representing pulleys, hooks, winches, trolley systems, etc., using kinematic constraints.

Requirement (i) can be met using a fixed integration step of

$\Delta t = 1/60$ s ≈ 16.67 ms, provided the computational time required to perform a single step is considerably smaller that Δt. Variable time step or multiple smaller steps are possible but only if the *total wall clock* computational time is still within Δt for all steps. Also, a higher order method might not be compatible with the discontinuities due to impacts or dry friction, and this is another reason to prefer one-step, single-stage, fixed-step integration strategies. Requirement (ii) can be met by using a variational integrator [18] and in view of requirement (i), a first order method should be chosen. When constraints are used, either a mixed strategy [20] or a purely variational strategy [21] can be used, as long as it includes physical constraint relaxation and stabilization. These integration methods of Lacoursière make it possible to meet requirement (iv) as well. In this paper we use a somewhat simplified integration method which is not fully symplectic for non-zero relaxation. For zero relaxation, our method reduces to the SHAKE [14] integrator, which is symplectic. For non-zero relaxation however, the proposed integrator is slightly dissipative and the additional terms provide constraint stabilization with strong linear stability. In effect the integrator gives globally bound energy, as required. Using a lumped element model based on rigid bodies ensures compliance with requirement (vi).

The large mass ratio requirement (iii) is specific to hoisting cable. In combination with the requirement (v) of stiff elasticity, the equations of motion become particularly stiff and many of the methods widely used in computer graphics—spring-and-damper models in particular—are ruled out because of stability issues, or for lack of a direct correspondence between simulation parameters and physical properties. Since available VE frameworks largely build on efficient techniques for rigid body simulation, the requirements (i) and (vi) suggests that also cables should be modeled as lumped elements, using rigid body components.

B. Previous work

An overview of the dynamics and control of cranes is not presented here but is found in the literature [1]. When it comes to simulation, most common crane models do not include any dynamics for the cable. In some applications the cable is included as a single stiff spring of variable length or modeled by a single kinematic constraint between the load and the hoisting structure. In more elaborate models [15], [19] the hoisting dynamics is derived from a kinematic constraint acting simultaneously on the crane construction, trolleys, and loads, maintaining a given total length of the cable. We also extended such models in a previous paper [29] to include resistance to cable twisting motion and cable elasticity. In none of the strategies cited above is the cable represented by a physical body and thus, these do not allow full scale interaction between the cable and other objects in a VE *via* contacts, for instance.

There are few examples of real-time simulations for VEs involving *dynamics* cable models—presumably due to the difficulty in producing fast and stable simulations for these for large stiffness—and no examples of hoisting of *heavy* loads. Cables are examples of deformable physical bodies. These can be simulated using either *finite elements*, *lumped elements*, or *modal* models. Both lumped and finite element models have been used to simulate cables. A short review of these applications is now provided with an emphasis on models and methods which have been applied to interactive simulation.

A simulation model using finite elements [10] based on the Cosserat model, including stretching, torsional, and bending energy [26], was found to be efficient as long as connection points are restricted at the extremities of the cable, thus limiting interactivity.

Lumped element models couple simple physical bodies such as point particles or rigid bodies with penalty forces or constraints. A rigid body model was used for the simulation of antenna booms carried by space shuttles [7]. Systems of point masses connected with spring-damper forces have been reported, modeling either stretching [16], or both stretching and bending [23]. Note however that particle models do not allow torsion which is needed in the simulation of hoisting. Lumped point mass element models of Cosserat rods including stretching, bending and torsional elasticity has been presented in Refs. [13], [31]. The bending and torsion is included by augmenting the point mass system by assigning the intermediate segments a rotational state. This extends the system degrees of freedom to that of a cable modeled by lumped rigid bodies and the equations to be integrated in time are precisely the Newton-Euler equations of motion. These papers present no validation of the models or present performance of high mass ratios. There are also other strategies based on point particles and penalty forces proportional to displacements from a reference configuration, either by defining restoring forces for volume, surface, or linear distortion [28], [32], or using a global, co-rotated shape matching strategy [24]. Models based on penalty forces have limitations with regards to stiffness, however. This can be alleviated to some degree by using an implicit numerical integrator [25], though the computational cost for this is similar to that of solving for a constrained system.

Lumped elements can be coupled using kinematic constraints also. It is possible to simulate a perfectly rigid chain by connecting rigid bodies with hinges of alternating rotation axis for instance. Using standard methods of robotics [35], such a chain can be made perfectly rigid, and can be a good starting point for cable models of cranes [17]. The resulting cable is then perfectly inelastic however, and cannot account for stretching dynamics at all. If one uses a descriptor form of the constrained equations of motion (also referred to as the Lagrange multiplier method), solving explicitly for the constraint forces, exact constraint satisfaction can be relaxed. The descriptor formulation is advantageous because of the unified treatment of nonholonomic constraints and loop closure constraints. It has the same linear complexity as the recursive formulation of robotics for linear chains provided sparsity is exploited in the linear systems of equations. In addition, the descriptor formulation allows for constraint relaxation, which is not possible with recursive or reduced coordinate methods of robotics. However, using standard constraint stabilization techniques [3]–[5], [9], it is not possible to map the relaxation parameters to the physical parameters. This is remedied with the technique of §II.

Multibody systems subject to constraints are more expensive to simulate than those involving only explicit forces. Recent papers suggest that it is possible to achieve linear or even logarithmic complexity with enough parallelism [12], [27], by exploiting a level-of-detail strategy. A related method showing

linear complexity in both number of elements and number of contacts is presented in Ref. [34].

The difficulty in achieving stable real-time simulation including a dynamical cable model for hoisting of heavy weights (more than 10-100 times the cable mass) is not covered in any of the cited work above, because of limitations on stiffness or mass ratios. To our knowledge, there is no existing method that meets the requirements for hoisting cable in VEs listed in § I-A.

C. Our contributions

The contributions of this paper to the modeling and computation of cable dynamics for VEs are the following. We formulate a cable model as a chain of rigid bodies connected with a new type of *angular constraint*. This constraint is formulated in terms of the joint center, as well as the bend and twist angles about it. A regularization technique is used to allow constraint relaxation and to associate energy with constraint violation. In the stiff limit, the new constraint is just one form of *rigid locking*. However, the configuration is designed to parametrize the degrees of freedom as they appear in elasticity theory when the constraint is relaxed. This provides a direct connection to elasticity theory. With the chosen integration method, described in § II-B, the relaxation parameters can be safely set to zero, corresponding to rigid constraints. For nonzero relaxation, our experiments validate the model, as the force-displacement relations match those predicted by the theory.

We demonstrate the stability of the time stepping scheme of § II-B at step size $\Delta t = 1/60\ s$ and for mass ratios up to 10^5 for rigid body examples. Using a particle model that includes bending energies, the mass ratio can be arbitrarily high provided the bending energy is scaled adequately to suppress transversal high frequency oscillations. We argue that the bending and torsional forces have a stabilizing effect on the system, and we present an analysis of the mechanism at work here.

It should be emphasized that the elastic forces described cannot be included as explicit forces, but must be computed as regularized constraints in order to achieve stability for the range of parameters covered. Integration can be made efficient by recognizing the strongly banded structure of the Schur complement—the matrix involved in the linear equation to be solved at each time step. The remaining loop-closing constraints result in a few off-diagonal blocks. The system is solved using a block preconditioned Gauss-Seidel solver, where the cable block is solved using a direct fixed bandwidth solver, and the couplings between the cable and other objects are computed using Gauss-Seidel iterations. The computational performance of the simulation depends linearly on the number of cable elements. These operations are constructed to preserve the total linear and angular momentum and the local deformation energy.

Although we focus on hoisting cable, the method we present is of general use for the graphics community. Constraint regularization can improve the numerical stability of any simulation of systems with stiff interactions, and the angular constraint in particular can be applied to any (Cartesian-coordinate) constraint-based articulated body solver. The constraint method itself can handle branching and closed loops efficiently and with linear complexity provided a good sparse solver is used such as UMFPACK [33]. Finding an optimal strategy for closed loops is ongoing research and will be published elsewhere.

The rest of the paper is organized as follows. Essential notions of multibody dynamics in descriptor form are presented in § II, which contains the integration method in § II-B. Several alternative models to simulate cables with relaxed constraints are presented in § III and experiments are performed on these to determine the most stable ones. Elements of elasticity theory for cables are then presented in § IV. A preconditioned Gauss-Seidel solver which uses grouping and splitting, is then presented in § VI. Results of model validation and numerical stability experiments are presented in § VII. Example applications are discussed in § VIII, followed by a summary and conclusions in § IX.

II. Multibody dynamics

The following notations are used in what follows. Unless explicitly stated all quantities are expressed in a global inertial frame. The state vector of the multibody system of N rigid bodies is $(q^T, v^T)^T$. The partitioned vector $q = (q_{(1)}^T, q_{(2)}^T, \ldots, q_{(N)}^T)^T$ contains the generalized coordinate vectors $q_{(i)} = (\mathbf{x}_{(i)}^T, e_{(i)}^T)^T$, where $\mathbf{x}_{(i)}$ is the center of mass position vector of body (i) and $e_{(i)}$ is a unit quaternion defining the orientation of the body. The velocities are represented by $v = (v_{(1)}^T, v_{(2)}^T, \ldots, v_{(N)}^T)^T$, where $v_{(i)} = (\dot{\mathbf{x}}_{(i)}^T, \omega_{(i)}^T)^T$ for body (i) and with the angular velocity vector denoted by $\omega_{(i)}$. With these representations we have the relation $\dot{q}_{(i)} = T(q_{(i)})v_{(i)}$, where $T(q_{(i)}) = \mathrm{diag}(1_{3\times3}, \tilde{T}(e_{(i)}))$, $1_{3\times3}$ is the 3×3 identity matrix and

$$\tilde{T}(e) = \frac{1}{2}\begin{pmatrix} -e_1 & -e_2 & -e_3 \\ e_0 & e_3 & -e_2 \\ -e_3 & e_0 & e_1 \\ e_2 & -e_1 & e_0 \end{pmatrix} \tag{1}$$

The body mass $m_{(i)}$ and inertia tensor $I_{(i)}$, expressed in the inertial frame, are collected into the mass matrix $M_{(i)} = \mathrm{diag}(m_{(i)}1_{3\times3}, I_{(i)})$. The mass matrix of the entire system is then $M = \mathrm{diag}(M_{(1)}, M_{(2)}, \ldots, M_{(N)})$. The body frame inertia tensor is $I_{(i)}^0$ so the inertia tensor in the inertial frame is $I_{(i)} = R_{(i)}I_{(i)}^0R_{(i)}^T$, where $R_{(i)} = R_{(i)}(e_{(i)})$ is the rotation matrix of body (i).

The multibody system then satisfies the Newton-Euler equations of motion

$$M\dot{v} = f_M + f, \tag{2}$$

where f represents internal and external forces and $f_M = -\dot{M}v$ is the gyroscopic force. For each rigid body (i) we can read off the equation $M_{(i)}\dot{v}_{(i)} = f_{M_{(i)}} + f_{(i)}$, where $f_{M_{(i)}} = -\dot{M}_{(i)}v_{(i)}$. The Newton-Euler equations are discretized and integrated to produce the discrete trajectories at fixed time intervals[1]. These are then used to drive the 3D graphics display.

A. Potentials and constraints

The internal interactions are modeled with potential forces and kinematic constraints. The potential energy of the system is $U(q,t)$ and the corresponding force is $f = -T^T\partial U/\partial q^T$.

[1] An alternative approach is to make a time discretization of the Lagrangian for the system and impose a discretized least action principle. Numerical integrators derived this way are referred to as variational integrators and these can be constructed to preserve invariants of the system. See Ref. [18] for further details.

For stiff systems, subject to strong elastic and dissipative forces varying significantly on comparatively short time scales, it is particularly difficult to find numerical integrators that are fast, stable, and faithful to the physics. As an alternative approach to standard implicit integration, strong forces are here considered as weakly relaxed kinematic constraints—a form of regularization. Mathematically, a constraint restricts the coordinates to lie on a surface $\phi(q,t) = 0$ in configuration space. That surface can be time dependent. The corresponding constraint force which acts to keep the coordinates $q(t)$ on the surface $\phi(q,t) = 0$, is $f_c = J^T\lambda$, where $J = (\partial\phi/\partial q)T(q)$ is the constraint Jacobian and λ, the Lagrange multiplier. The constraint force acts in a direction normal to the constraint surface. The constraint force amplitude λ is here seen as dynamical variable and the equations of motion are no longer a set of ordinary differential equations (ODE), but instead, they form a set of differential algebraic equations (DAEs) with the inclusion of the algebraic equation $\phi(q,t) = 0$. Differentiating the constraint $\phi(q,t) = 0$ with respect to time yields $0 = \dot{\phi} = Jv + \partial_t\phi$. Therefore, time-dependent constraints, assuming that $Jv = 0$, exert the instantaneous rate of work $f_c^T v = \lambda^T Jv = -\lambda^T(\partial\phi/\partial t)$ on the system.

For a system with N_c constraints, we use the representation $\phi = (\phi_{[1]}^T, \phi_{[2]}^T, \ldots, \phi_{[N_c]}^T)^T$, where $\phi_{[i]}$ is the ith constraint with dimension $d_{[i]}$, and involves any number of bodies. The dimension of ϕ is thus $\dim(\phi) = \sum_i d_{[i]} \equiv d_c$. The dimension of the system Jacobian is then $\dim(J) = d_c \times 6N$ and the dimension of the Lagrange multiplier is $\dim(\lambda) = d_c$.

Unless a coordinate reduction strategy is used, constraints are never exactly satisfied during numerical integration and the *constraint violation*—the Euclidean norm $|\phi|$—has a finite value and dynamics of its own. There are various well-known techniques to stabilize constraint violation [3]–[5], [9]. Our choice is a physical constraint regularization and stabilization scheme [20], in which constraints are made explicitly compliant and thus allowed to oscillate, and then strongly damped, using only physical terms added to the Lagrangian formulation. In this framework, constraints are replaced by stiff potentials but the DAE form of the system is retained so the variables λ are solved for directly and discretized independently of the other variables. We may represent the system potential as

$$U(q) = \tfrac{1}{2}\phi^T(q)\varepsilon^{-1}\phi(q) \tag{3}$$

for some real, non-negative, diagonal matrix ε, of dimension $d_c \times d_c$, that has the role of inverse stiffness of the potential. The contribution to the generalized force of this potential takes the form

$$f_\phi = -J^T\varepsilon^{-1}\phi \tag{4}$$

Note that if the artificial variable λ is introduced as $\lambda = -\varepsilon^{-1}\phi$ the generalized force can be written $f_\phi = J^T\lambda$ and the equations of motion are modified to the following DAE system

$$\dot{q} = T(q)v \tag{5}$$

$$M\dot{v} - J^T\lambda = f_M + f \tag{6}$$

$$\varepsilon\lambda(q,t) = -\phi(q,t). \tag{7}$$

In this formulation, we may choose between making the constraint entirely stiff by setting $\varepsilon = 0$ without any singularities in (5) and (7) or working with finite stiffness. A stiff force representation without the λ would not have a well behaved limit as $\varepsilon \to 0$. For finite regularization $\varepsilon > 0$, the constraint forces are linear restorations of stiffness $1/\varepsilon$, directly proportional to the constraint violation. Strong damping can also be added by substituting $\phi \to \phi + \beta\dot{\phi}$ in the right hand side of (7), with a damping coefficient $\beta > 0$. The effective damping coefficient for constraint oscillations is then β/ε, and this damping also behaves nicely as $\varepsilon \to 0$ when the discretization of §II-B is used.

B. Numerical integration

We use a mix of the *symplectic* and linearly implicit Euler methods for the numerical integration of the system of (5)–(7). The symplectic Euler method, also known as Störmer-Verlet, has good properties with respect to global preservation of the invariants of physical systems [14]. This makes it a natural choice when symplecticity and preservation of global invariants are of higher importance than high local accuracy. Symplectic Euler is used for the dynamics variable on the first line of the equations of motion (5). The second line is the discretized using the implicit Euler formula of first order because that equation is assumed to be stiff. The same combination was used in the context of real-time simulation of deformable bodies previously [30].

Symplectic Euler discretization of the system (5)–(7) and Taylor expansion $\phi(x_{n+1}) = \phi_n + \Delta t J_n v_{n+1} + O(\Delta t^2)$ gives the following first order time stepping algorithm

$$q_{n+1} = q_n + \Delta t T(q_n) v_{n+1} \tag{8}$$

$$A_n u_{n+1} = b_n, \tag{9}$$

where

$$A_n = \begin{pmatrix} M_n & -J_n^T \\ J_n & \Delta t^{-2}\varepsilon \end{pmatrix}, \tag{10}$$

and $u_{n+1} = (v_{n+1}^T, \Delta t\lambda_{n+1}^T)^T$, $b_n = (Mv_n^T + \Delta t f_n^T, -\Delta t^{-1}\phi_n^T)^T$ and the gyroscopic force f_M is included in f from here on. The matrix A_n is typically block sparse. The linear system of equations may be solved by first building the Schur complement, $S \equiv JM^{-1}J^T + \Delta t^{-2}\varepsilon$, solve for the Lagrange multiplier from

$$S\lambda = -\Delta t^{-1}Jv - JM^{-1}f - \Delta t^{-2}\phi \tag{11}$$

and then compute the velocity v_{n+1} by direct substitution and finally update the positions. Observe that there is no singularity for $\varepsilon = 0$, which can be made arbitrarily small, as long as the Jacobian matrix J has full row rank. In addition, for finite $\varepsilon > 0$, the linear system is well posed, and it is well conditioned as long as the rows of J and M are not badly scaled.

III. Numerical stability experiments of particle-based cables

The double pendulum is well-known to become numerically ill-conditioned for large mass ratios. We thus investigate how the N-link pendulum may be stabilized by adding supplementary constraints between heavy or static components and lighter elements. An illustration of the configurations considered in the following numerical experiments is found in Fig. 1. Of course, regularization can be applied to any of the different models. The main question we strive to answer here is whether stability can be increased by simultaneously relaxing constraints coupling the lighter elements, and strengthening the constraints between the

heavier ones, usually found at each end of a cable. The physical idea behind this is to let constraints between elements of similar mass take most of the heavy load. Numerically, this corresponds to equilibrating the scaling of the rows of the Schur complement matrix, S.

The reason for performing numerical experiments to evaluate stability is that we suspect that constraints nonlinearity and finite precision arithmetic play determining roles, and neither issues are addressed satisfactorily with a linear stability analysis. For the systems at hand, the N particles are indexed by i. The heavy load has index $i = N$ and mass $M_i = \mathscr{M}$ and the light elements have index $i < N$ and mass $M_i = m$. The rest state separation length between the particles are denoted by d and the total length is $L = Nd$. The models considered are illustrated in Fig. 1 and the constraints for each case are as follows.

(a) Link chain (pair-wise distance constraints)

$$\begin{aligned}\phi &= (\phi_{d0}, \ldots, \phi_{dN-1})^T,\\ 0 &= \phi_{di} \equiv |\mathbf{d}_i| - d;\end{aligned}$$

(b) Link chain enforced by a *massless cable constraint* [29] (a total length preservation constraint)

$$\begin{aligned}\phi &= (\phi_{d0}, \ldots, \phi_{dN-1}, \phi_m)^T,\\ 0 &= \phi_{di} \equiv |\mathbf{d}_i| - d,\\ 0 &= \phi_m \equiv \sum_{i=1}^{N} |\mathbf{d}_i| - L;\end{aligned}$$

(c) Link chain with *load enforcement* (an extra link for direct support of the load)

$$\begin{aligned}\phi &= (\phi_{d0}, \ldots, \phi_{dN-1}, \phi_{le})^T,\\ 0 &= \phi_{di} \equiv |\mathbf{d}_i| - d,\\ 0 &= \phi_{le} \equiv |\mathbf{x}_{(N)}| - L;\end{aligned}$$

(d) Truncated link chain enforced by a *massless cable constraint* (the bottom most link being removed)

$$\begin{aligned}\phi &= (\phi_{d0}, \ldots, \phi_{dN-2}, \phi_m)^T,\\ 0 &= \phi_{di} \equiv |\mathbf{d}_i| - d,\\ 0 &= \phi_m \equiv \sum_{i=1}^{N} |\mathbf{d}_i| - L;\end{aligned}$$

(e) Link chain with *angular constraint* (the chain link kept at straight angles)

$$\begin{aligned}\phi &= (\phi_{d0}, \phi_{a0}^T, \ldots, \phi_{dN-2}, \phi_{aN-2}^T, \phi_{dN-1})^T,\\ 0 &= \phi_{di} \equiv |\mathbf{d}_i| - d,\\ 0 &= \phi_{ai} \equiv \arctan(|\mathbf{d}_i \times \mathbf{d}_{i+1}|, \mathbf{d}_i \cdot \mathbf{d}_{i+1});\end{aligned}$$

where $\mathbf{d}_i = \mathbf{x}_{(i+1)} - \mathbf{x}_{(i)}$ and $\mathbf{x}_{(0)}$ is the constant position of the pendulum anchor point. We use the arctan 2 function such that the bend angle, ϕ_{ai}, ranges between $(-\pi, \pi)$. The Jacobian blocks are

$$J_{dii} = -J_{diii+1} = \frac{-\mathbf{d}_i}{|\mathbf{d}_i|}, \tag{12}$$

$$J_m = \sum_{i=1}^{N} \left(\ldots, \frac{\mathbf{d}_i}{|\mathbf{d}_i|}, \ldots, \frac{-\mathbf{d}_i}{|\mathbf{d}_i|}, \ldots \right), \tag{13}$$

$$J_{ai} \equiv (J_{aii}, J_{aii+1}, J_{aii+2}) = \frac{d_\cdot}{d_\times^2 + d_\cdot^2} \mathscr{A} - \frac{|\mathbf{d}_\times|}{d_\times^2 + d_\cdot^2} \mathscr{B}, \tag{14}$$

TABLE I

THE MAXIMUM MASS RATIO $\mathscr{M}/m$ IS DETERMINED FROM NUMERICAL EXPERIMENTS OF THE DIFFERENT MODELS AND REGULARIZATION PARAMETERS FOR STRETCHING, ε_d, AND SUPPLEMENTARY CONSTRAINT, ε_x (BEING EITHER OF ε_m, ε_{le} AND ε_a).

Model	ε_d (m/N)	ε_x (m/N)	$(\mathscr{M}/m)_{max}$
a)	10^{-8}		10^2
b)	10^{-8}	10^{-9}	10^2
c)	10^{-8}	10^{-9}	10^3
c)	10^{-8}	10^{-12}	$\mathbf{10^7}$
c)	10^{-18}	10^{-22}	$\mathbf{10^{15}}$
d)	10^{-8}	10^{-9}	10^2
e)	10^{-8}	10^{-4}	10^3
e)	10^{-11}	10^{-9}	$\mathbf{10^7}$
e)	10^{-18}	10^{-17}	$\mathbf{10^{15}}$

where

$$\mathscr{A} = |\mathbf{d}_\times|^{-1}(\mathbf{d}_\times \times \mathbf{d}_{i+1}, -\mathbf{d}_\times \times [\mathbf{d}_i + \mathbf{d}_{i+1}], \mathbf{d}_\times \times \mathbf{d}_i), \tag{15}$$

$$\mathscr{B} = (-\mathbf{d}_{i+1}, \mathbf{d}_{i+1} - \mathbf{d}_i, \mathbf{d}_i), \tag{16}$$

and $\mathbf{d}_\times = \mathbf{d}_i \times \mathbf{d}_{i+1}$ and $d_\cdot = \mathbf{d}_i \cdot \mathbf{d}_{i+1}$. The dimension of J_{ai} in this case is 1×9, i.e., it contains three 1×3 block element contributions to the full Jacobian.

We regularize the constraints, thus introducing elasticity in the system, and integrate the system using the integrator presented in Sec. II-B. A relaxation parameter ε_d, ε_m, ε_{le} and ε_a, are introduced for each constraint. A chain of 5 links ($N = 5$) is dropped from rest in horizontal position with gravity set to $G = 10\ m/s^2$. The light mass is set to $m = 1\ kg$ and the system is integrated with time step $\Delta t = 1/60\ s$. Instabilities are identified by large, or even diverging, variations in ϕ_{di}. These variations are computed for different mass ratios $\mathscr{M}/m$. The results are displayed in Tab. I. The dependence on the number of links N in these experiments is weak, and increasingly so with increasing mass ratio.

As expected, the ordinary chain link model, model (a), becomes numerically unstable already for moderate mass ratios, $\mathscr{M}/m = 100$. This holds irrespective of whether the stretch stiffness, ε_d^{-1}, is small or large. The same holds also for the chain link enforced by a massless cable (model (b)) and the same model with the bottom link truncated (model (d)). These extensions *do not* increase the numerical stability irrespectively of the stiffness values of the massless cables. We conclude that replacing the gravitational support of the load, from the stiff distance constraints, with a stiff massless cable, simultaneously softening the distance constraints, do not improve the numerical stability. On the other hand, adding a supplementary distance constraint between the heavy load and the supporting element directly, without coupling it to any of the light masses—model (c)—*does* increase stability. For this case, the simulations are well behaved for mass ratios well beyond practical use, up to $\mathscr{M}/m = 10^{15}$, and using regularization parameter $\varepsilon_{le} = 10^{-22}\ m/N$. Surprisingly, introducing an angular constraint—as in model (e)—yields similar stability. Model (e) is stable for mass ratios up to $\mathscr{M}/m = 10^{15}$, with angular regularization parameter $\varepsilon_a = 10^{-17}\ rad/N$. The importance of this result lies in that the chain link system with regularized angular constraint is not only numerically stable but also a *practically useful model* since it allows deformations, vibrations, and slacking, as might happen in response to other interactions. This contrasts with model (c) where bending deformations conflict

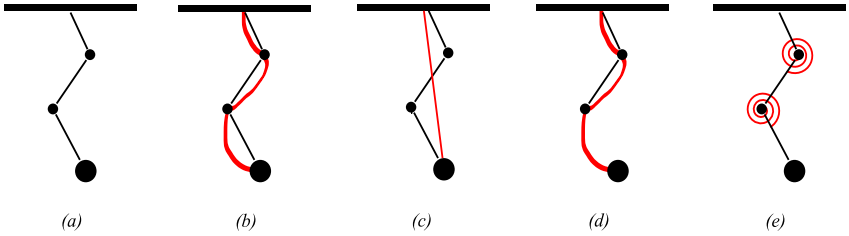

Fig. 1. Illustration of the link chain configurations considered. The red curve represents constraints supplementary to the pairwise distance constraints. The purpose of the supplementary constraints are to increase the numerical stability of the system. These supplementary constraints are massless cable, model (b)-(d), and angular constraint, model (e).

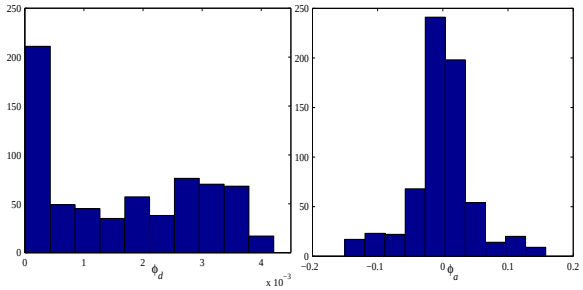

Fig. 2. The distribution of ϕ_d and ϕ_a sampled over time for a chain link system (model (a)). The strongest concentrations are at $\phi_d = 0$ and $\phi_a = 0$.

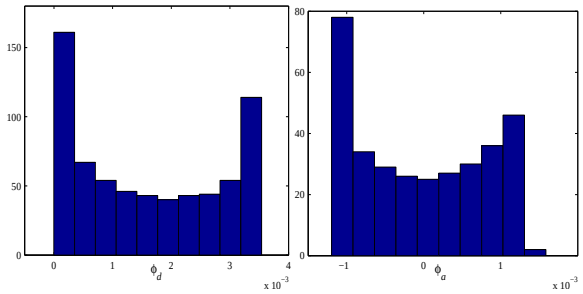

Fig. 3. The distribution of ϕ_d and ϕ_a sampled over time for a chain link system with angular constraint (model (e)). The magnitude of ϕ_a is diminished and the distributions becomes bi-valued.

with the stabilizing constraint, limiting interactions with the rest of the scene.

Three types of data are sampled and further analyzed in order to understand the mechanism behind the increased numerical stability. We plot ϕ_d and ϕ_a in Fig. 2 (model (a)) and 3 (model (e)) for the top most particle sampled in a simulation of a five link system with mass ratio $\mathscr{M}/m = 100$. The cable stretch parameter is $\varepsilon_d = 10^{-6}$ m/N and the bend parameter $\varepsilon_a = 10^{-4}$ rad/N. The system is integrated with time step $\Delta t = 1/60$ s over 30 s (6 turns). For the chain link system shown in Fig. 2, we have strongest concentrations at $\phi_d = 0$ and $\phi_a = 0$. The effect of the angular constraint, seen in Fig. 3 is clearly a large decrease in the magnitude of ϕ_a and a minor decrease if ϕ_d. The bending resistance also makes the distributions of ϕ_d and ϕ_a bi-valued. This means that the cable in this case spends more time being bent than straight.

The *return maps* of ϕ_d are then shown in Fig. 4 for the model (a) and model (e). This is a plot of $\phi_d(t)$ versus $\phi_d(t+\Delta t)$ and is a form of discrete phase plot. For model (a), the return

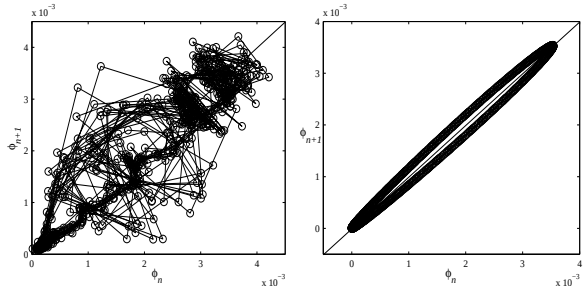

Fig. 4. The return map for a chain link system (model (a) in the left figure) versus a chain link system with angular constraint (model (e) in the right figure).

map is irregular and $\phi_d(t)$ is nearly uncorrelated with $\phi_d(t+\Delta t)$, showing evidence of high frequency, chaotic motion. For model (e) however, the return map is an ellipse, indicating simple harmonic motion of low frequency.

Finally, a spectral analysis of time series of ϕ_d for model (e) is shown in Fig. 5, for three values of ε_a, namely, $10^{-1}, 5 \cdot 10^{-3}, 10^{-4}$ rad/N. For $\varepsilon_a = 10^{-1}$ rad/N the system is essentially equivalent to the ordinary chain link system, model (a). The spectral distributions clearly shows how the oscillation modes of the system are suppressed and driven toward lower frequency with decreasing value on ε_a, corresponding to increasing bending resistance. In this simulation we used stretch stiffness $\varepsilon_d = 10^{-6}$ m/N and mass ratio $\mathscr{M}/m = 150$. Both models are stable in this case though model (a) is close to instability.

A schematic illustration composed from the stability data is found in Fig. 6. What is happening here is that for the ordinary chain link, model (a), there is nothing that prevents transverse oscillations of the particles, at least to first order. Transverse displacement produce only second order longitudinal displacement, and only second order response from the distance constraint and the gravitational pull. This system therefore exhibits high frequency oscillations in the transverse direction, which develop into numerical instabilities. *By introducing bending deformation forces, short wave length oscillations are suppressed and the system is driven toward slow coherent long wavelength vibrations and is thereby stabilized.* It should be emphasized that the stabilizing bend force cannot be included as an explicit force in the system but must be computed as a regularized constraint to have this effect. We expect that these results also apply to rigid body based cable.

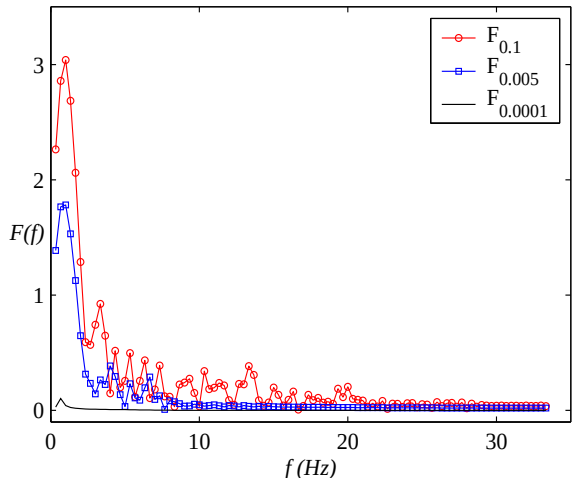

Fig. 5. The distribution functions of vibrational frequencies for model (e) obtained from Fourier analysis of the bend angle over time. The results come from simulations with varying bending stiffness $\varepsilon_s = 0.1$ (red line), $\varepsilon_s = 0.005$ (blue line), $\varepsilon_s = 10^{-4}$ (black line). Clearly increasing bending resistance diminishes the spectrum of vibrations.

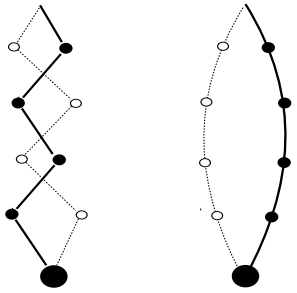

Fig. 6. The regularized angular constraint introduces resistance to bending. This suppresses short wave length oscillations (left figure) in favor for long wave length oscillations (right figure). As a result there are less high frequency oscillation modes that may develop numerical instabilities.

IV. Elasticity theory for cables

We consider a cable that can be modeled using the *Cosserat theory*, based on elastic rods [2]. This implies that the width of the cable is much smaller than the characteristic length scale of deformations. The simplest constitutive model is chosen, namely, the Kirchhoff relations. This corresponds to Hooke's linear law generalized to 3-dimensional curves. A general deformation is a combination of *stretching* or tangential deformations, *bending* or curvature deformations, and *torsion* or twisting deformations, as shown in Fig 7. The resulting stresses depend on the material parameters, namely, Young's modulus Y and Poisson's ratio σ. The deformation energy for a cable of length L is $U = U_s + U_b + U_t$, where

$$U_s = \tfrac{1}{2} c_s \delta x^2, \tag{17}$$

$$U_b = \tfrac{1}{2} c_b \kappa^2, \text{ and} \tag{18}$$

$$U_t = \tfrac{1}{2} c_t \Omega^2, \tag{19}$$

and δx is the elongation, κ is the curvature ($\kappa = R^{-1}$, with radius of curvature R) and twist angle Ω. The constants c_s, c_b, c_t play the role of stiffness coefficients and are $c_s = YA/L$, $c_b = YI_AL$ and $c_t = YI_A/2(1+\sigma)L$, where A is the cross-section area, and I_A is the area's moment of inertia along the central axis normalized by mass. This is $A^2/12$ for a quadratic cross-section.

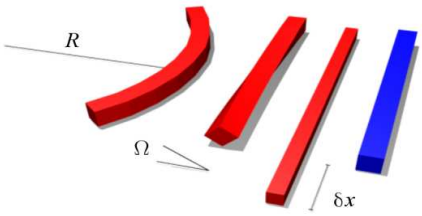

Fig. 7. The three types of deformation for a rod: stretching by a length δx, twisting by an angle Ω and bending with a radius of curvature R.

V. A rigid body-based model for cables

The rigid-body cable model consists of N rigid bodies connected in a chain by $N_C = N-1$ constraints as shown in Fig. 8. Inspired by the results shown in § III, a special *angular constraint* is introduced. This constraint is designed to parametrize geometric stretching, bending and torsion between pairs of bodies in a way that is compatible with the elasticity theory of § IV. When this constraint is regularized, physics motivated elasticity is introduced in the cable. The regularization parameters then corresponds to stretching, bending, and torsional stiffnesses. It should be emphasized that regularization of the conventional lock constraint based on direction cosines between body-fixed vectors has several drawbacks. First, it does not provide a correct measure for the amount of deformation at large angles and second, there is ambiguity with several local minima that causes the force to flip in direction at certain angles.

A. The angular constraints

The cable constraint vector is $\phi = (\phi_{[1]}^T, \phi_{[2]}^T, \ldots, \phi_{[N_c]}^T)^T$. Each angular constraint $[i]$ couples body (i) to body $(i+1)$, see Fig. 8.

For handling large deformation the constraint must be formulated directly in terms of angles, *not* direction cosines. We introduce body fixed vectors $\mathbf{d}_{(i)} = \mathbf{u}_{(i)}$, that represents the local cable axis at body i, and body-fixed vectors $\tilde{\mathbf{d}}_{(i,i)} = \mathbf{v}_{(i)}$ and $\tilde{\mathbf{d}}_{(i,i+1)} = \mathbf{w}_{(i+1)}$ that are mutually perpendicular to $\mathbf{d}_{(i)}$ and $\mathbf{d}_{(i+1)}$, respectively.

The angular constraint is formulated as

$$0 = \phi_{[i]} \equiv \begin{pmatrix} \phi_p \\ \phi_b \\ \phi_t \end{pmatrix} \equiv \begin{pmatrix} \mathbf{p}_{(i,i+1)} - \mathbf{p}_{(i+1,i)} \\ \theta_{[i]} \\ \Omega_{[i]} \end{pmatrix}. \tag{20}$$

The first three-dimensional component of the constraint corresponds to a *spherical* or *ball and socket* constraint, defined from body-fixed attachment points $\mathbf{p}_{(i,i+1)}$ and $\mathbf{p}_{(i+1,i)}$, expressed in the inertial frame. In terms of body center of mass $\mathbf{x}_{(j)}$ and attachment point $\mathbf{r}_{(i,j)}$ relative to body center of mass we have $\mathbf{p}_{(i,i+1)} = \mathbf{x}_{(i)} + \mathbf{r}_{(i,i+1)}$. The spherical constraint prevents stretching of the cable. The constraint $\phi_b \equiv \theta = 0$ produces a hinge about the cable axis—and results in bending resistance after regularization. The constraint $\phi_t \equiv \Omega = 0$ restricts rotation about the cable axis and

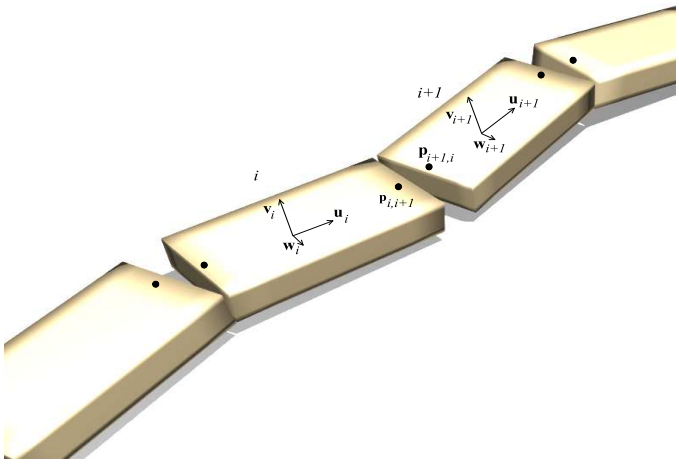

Fig. 8. The angular constraint is formulated in terms of body fixed anchor points and direction vectors illustrated in this figure.

produces twist force. The bend and twist angles are computed as

$$\theta_{[i]} = \arctan\left[|\mathbf{d}_{(i)} \times \mathbf{d}_{(i+1)}|/(\mathbf{d}_{(i)} \cdot \mathbf{d}_{(i+1)})\right], \tag{21}$$

$$\Omega_{[i]} = \arctan\left[|\tilde{\mathbf{d}}_{(i,i)} \times \tilde{\mathbf{d}}_{(i,i+1)}|/(\tilde{\mathbf{d}}_{(i,i)} \cdot \tilde{\mathbf{d}}_{(i,i+1)})\right] - \pi/2 + 2\pi\eta, \tag{22}$$

where the angles are computed using `arctan2` such that the angles ranges between $-\pi$ to π and η is the winding number. The term $-\pi/2$ is due to that the vectors $\tilde{\mathbf{d}}_{(i,i)}$ and $\tilde{\mathbf{d}}_{(i,i+1)}$ are perpendicular in the rest configuration. An alternative angular constraint may be constructed by setting $\tilde{\mathbf{d}}_{(i,i)} = \mathbf{v}_{(i)}$ and $\tilde{\mathbf{d}}_{(i,i+1)} = \mathbf{v}_{(i+1)}$, which are co-aligned in the rest state, and dropping the term $-\pi/2$ in (22). This formulation has the drawback that the twist angle, Ω, measures also bending deformations. When there is no bending deformations, Ω measures the twist angle exactly. But when the deformation is a combination of twisting and bending, we get an extra contribution $\Omega \to \Omega + \theta$ resulting in an extra contribution to the bend force. If $c_b \gg c_t$ this error is negligible though. As we shall see, this alternative formulation has superior stability properties in the large mass-ratio regime.

We identify the Jacobian by differentiating ϕ in combination with the fact that $0 = \dot{\phi} = Jv$. For a cable system the Jacobian has the form

$$J = \begin{pmatrix} J_{(1,1)} & J_{(1,2)} & & & \\ & J_{(2,2)} & J_{(2,3)} & & \\ & & \ddots & & \\ & & & J_{(N_C,N_C)} & J_{(N_C,N_C+1)} \end{pmatrix}, \tag{23}$$

where the sub-block Jacobians are[2]

$$J_{(i,i)} = \begin{pmatrix} 1_{3\times3} & r^*_{(i,i)} \\ 0_{1\times3} & \mathscr{A}^T_{(i)} \\ 0_{1\times3} & \mathscr{B}^T_{(i)} \end{pmatrix}, \tag{25}$$

[2]The time derivative of the arctan function $f(t) = \arctan(x(t)/y(t))$ is

$$\dot{f} = \frac{1}{x^2+y^2}\left[y\dot{x} - x\dot{y}\right], \tag{24}$$

$$J_{(i,i+1)} = -\begin{pmatrix} 1_{3\times3} & r^*_{(i,i+1)} \\ 0_{1\times3} & \mathscr{A}^T_{(i)} \\ 0_{1\times3} & \mathscr{B}^T_{(i)} \end{pmatrix}. \tag{26}$$

The 3×3 matrix $r^*_{(i,j)}$ is the skew-symmetric matrix corresponding to vector $\mathbf{r}_{(i,j)}$ and

$$\mathscr{A}_{(i)} \equiv -\frac{1}{d_\times^2 + d_\cdot^2}\left[d_\times + \frac{d_\cdot^2}{d_\times}\right]\mathbf{d}_\times \tag{27}$$

$$\mathscr{B}_{(i)} \equiv -\frac{1}{\tilde{d}_\times^2 + \tilde{d}_\cdot^2}\left[|\tilde{d}_\times| + \frac{\tilde{d}_\cdot^2}{|\tilde{d}_\times|}\right]\tilde{\mathbf{d}}_\times \tag{28}$$

where $\mathbf{d}_\times = \mathbf{d}_{(i)} \times \mathbf{d}_{(i+1)}$, $\tilde{\mathbf{d}}_\times = \tilde{\mathbf{d}}_{(i,i)} \times \tilde{\mathbf{d}}_{(i,i+1)}$, $d_\times = |\mathbf{d}_\times|$,$\tilde{d}_\times = |\tilde{\mathbf{d}}_\times|$, $d_\cdot = \mathbf{d}_{(i)} \cdot \mathbf{d}_{(i+1)}$, and $\tilde{d}_\cdot = \tilde{\mathbf{d}}_{(i,i)} \cdot \tilde{\mathbf{d}}_{(i,i+1)}$. Observe that the sub-block Jacobian $J_{(i,j)}$ has dimension 5×6. The Jacobian has a singularity at $d_\times = 0$. This singularity is avoided by substituting $d_\times^{-1}$ with $(\varepsilon_0 + d_\times)^{-1}$ for some very small positive number ε_0.

B. The Schur complement

The first term in the Schur complement, S, introduced in (11), for a cable system is

$$JM^{-1}J^T = \begin{pmatrix} A_{[1]} & B_{[1]} & & \\ C_{[1]} & A_{[2]} & B_{[2]} & \\ & C_{[2]} & \ddots & \\ & & & A_{[NC]} \end{pmatrix} \tag{29}$$

with

$$A_{[i]} = J_{(i,i)}M^{-1}_{(i)}J^T_{(i,i)} + J_{(i,i+1)}M^{-1}_{(i+1)}J^T_{(i,i+1)} \tag{30}$$

$$B_{[i]} = J_{(i,i+1)}M^{-1}_{(i+1)}J^T_{(i+1,i+1)} \tag{31}$$

$$C_{[i]} = J_{(i+1,i+1)}M^{-1}_{(i+1)}J^T_{(i,i+1)} \tag{32}$$

The dimension of $A_{[i]}, B_{[i]}, C_{[i]}$ is 5×5. The total dimension of $JM^{-1}J^T$ for a cable system is $5N_C \times 5N_C$

C. Modeling elasticity with regularized constraints

We introduce elasticity in the system through constraint regularization

$$\phi \rightarrow U = \frac{1}{2}\phi^T(q)\varepsilon^{-1}\phi(q) \tag{33}$$

with $\mathrm{diag}(\varepsilon) = \mathrm{diag}(\varepsilon_{[1]}^T, \varepsilon_{[2]}^T, \ldots, \varepsilon_{[N_c]}^T)$ and $\varepsilon_{[i]} = \mathrm{diag}(\varepsilon_s, \varepsilon_s, \varepsilon_s, \varepsilon_b, \varepsilon_t) = \mathrm{diag}(c_s^{-1}, c_s^{-1}, c_s^{-1}, c_b^{-1}, c_t^{-1})$. For a constraint with two neighboring elements a and b having length $L_{(a)}$ and $L_{(b)}$ we have the following coefficients

$$c_s = \frac{YA}{L_{(a)} + L_{(b)}} \tag{34}$$

$$c_b = \frac{YI_A}{L_{(a)} + L_{(b)}} \tag{35}$$

$$c_t = \frac{YI_A}{2(1+\sigma)(L_{(a)} + L_{(b)})} \tag{36}$$

where we have made the transformation from curvature $\kappa = 1/R$ to bend angle θ as the measure for bending, for which the *local* bend energy reads $U_b = (1/2)c_b\theta^2$ when we assume locally small bend angles such that $\kappa \approx \theta/(L_{(a)} + L_{(b)})$. As we have a well defined measure for the bend angle, the method can handle large deformations. Although the linear force model is questionable in this regime, it is straight forward to extend this model to energies valid for large bend angles, i.e., by replacing $\phi = \theta$ with some more general, non-linear, function $\phi(\theta)$.

D. Contacts

An impulse-based method was used to handle colliding and continuous contacts in which penetrations were eliminated by iterative projections. A simple Coulomb friction model was also applied. To make the collision and contact models consistent with constraint based interactions, the impulses are treated as discrete forces, integrated over a time step. In production code, the contact impulses should be an integrated part of an iterative solver or introduced on the constraint level, in which case the problem of computing the constraint forces from (10), extends to a linear complementarity problem [20].

VI. The linear solver

We assume now that there is a large number of bodies and a corresponding large number of constraints. For structures with tree-like topology, there exist methods for which the computational time scales linearly, $O(N_c)$, with the number of bodies and constraints [8], [35]. But when the topology of the constraints includes closed kinematic loops it is more difficult to find efficient numerical algorithms, especially when contacts are considered. If a direct matrix solver with dense matrix representation is applied to (11) the computational time scales as $O(N_c^3)$. Many systems in VEs have *almost* tree structure topology with only a few closed loops because of constraints interconnecting more than two bodies, as is the case for the *massless cable strategy* [29]), or because of contacts and collisions. A preconditioned Gauss-Seidel algorithm that is easy to implement but a good compromise for the case at hand is now presented. In particular, this solver is shown to scale linearly with the number of cable elements and to provide solutions that are accurate enough for the mass ratios considered.

A. Groups of constraints

We split the constraints into groups as

$$\phi = \begin{pmatrix} \phi_\alpha(q_a, q_b, \ldots) \\ \phi_\beta(q_c, q_d, \ldots) \\ \vdots \\ \phi_i(q_a, q_b, q_c, q_d, \ldots) \end{pmatrix}, \tag{37}$$

where ϕ_α is the constraint vector for a group of bodies $(a, b, \ldots)$ with no closed loops (e.g., a cable) and ϕ_β a group of constraints and bodies $(c, d, \ldots)$ with *no* common members to the previous group, etc., The grouping of constraints and bodies are chosen so to form a minimum number of groups with tree-topology. In ϕ_i we collect constraints for interaction between the groups and loop-closing constraints.

The Jacobian has the form, after appropriate re-numbering of the bodies,

$$J = \begin{pmatrix} J_\alpha & & \\ & J_\beta & \\ & & \ddots \\ \cdots & J_i & \cdots \end{pmatrix} \tag{38}$$

For the Schur complement matrix in (11), this means

$$S \equiv JM^{-1}J^T + \Delta t^{-2}\varepsilon = \begin{pmatrix} S_{\alpha\alpha} & & & S_{\alpha i} \\ & S_{\beta\beta} & & S_{\beta i} \\ & & \ddots & \vdots \\ S_{i\alpha} & S_{i\beta} & \cdots & S_{ii} \end{pmatrix} \tag{39}$$

where $S_{xy} \equiv \bar{J_x}M^{-1}\bar{J_y^T} + \Delta t^{-2}\varepsilon_x\delta_{xy}$ with $x, y \in \alpha, \beta, \ldots, i$, $\bar{J_x}$ denotes the full Jacobian with all blocks zero besides the sub Jacobian J_x and δ_{xy} is non-zero and equal to the identity matrix if $x = y$. The Lagrange multiplier is $\lambda = (\lambda_\alpha^T, \lambda_\beta^T, \ldots, \lambda_i^T)^T$.

B. Solver strategy

Gauss-Seidel iterations are performed at the constraint group level. Each group of constraints is solved using a direct method, taking advantage of the narrow main-diagonal bandwidth structure in each sub-system. The reason for choosing the Gauss-Seidel algorithm is that it is simple to implement and when the system has topology close to tree-like with a few closing loops, it converges rather rapidly. The solver algorithm for the complete system is given in Algorithm 1.

VII. Results

Numerical experiments were performed to validate the physical behavior of the proposed model, verify numerical stability, and test the performance. The numerical code is an implementation of the rigid body cable model developed in § V and following Algorithm 1.

A. Model validation

We begin with numerical experiments to validate the physical behavior of the cable model. The theoretical relations between applied forces and geometrical deformation can be found in, e.g.,

Algorithm 1 Time stepping the system

Accumulate external forces
Compute impulses and accumulate collision forces, make position projections
Accumulate gyroscopic force
Compute and accumulate constraint forces:
loop {group α of constraints}
  compute sub-block Jacobian J_α and Schur complement blocks $S_{\alpha\alpha}$ and $S_{\alpha\beta}$ etc.
  compute trial solution λ_α^0 from $S_{\alpha\alpha}\lambda_\alpha^0 = b_\alpha$
end loop
loop {N_{it} times or until convergence}
  loop {group α of constraints}
    Build $L_\alpha = -\sum_{\beta<\alpha} S_{\alpha\beta}\lambda_\beta^{n+1}$
    Build $U_\alpha = -\sum_{\beta>\alpha} S_{\alpha\beta}\lambda_\beta^{n}$
    Solve $S_{\alpha\alpha}\lambda_\alpha^{n+1} = b_\alpha + L_\alpha + U_\alpha$
  end loop
end loop
Accumulate constraint forces $f_\alpha = J_\alpha^T \lambda_\alpha$
Step velocities and positions using symplectic Euler
Adapt the level of detail—merge/split bodies
Feed the new state to the viewer

Fig. 9. Snapshots from numerical experiment with bending and twisting deformations.

Ref. [22]. The experiments are *stretching*, *twisting* and *bending*. These experiments are conducted on a cable of length $L = 10$ *m*, with rectangular cross section area $A = 10^{-2}$ m^2, lumped into $N = 3, 6, 12, 24$ rigid segments and for the material parameters of rubber, nylon and steel ($Y = 2\cdot 10^7,\ 2\cdot 10^9,\ 2\cdot 10^{11} N/m^2$). The Poisson ratio is set to 0.3. Snapshot from the twisting and bending experiments are found in Fig. 9.

Results of the pull experiment are found in Fig. 10. This tests the theoretical relation $f/YA = \Delta L/L$, where f is a force pulling in the ends and directed outward. We note that the curve coincides well with theory and that there is no dependence on the spatial discretization, i.e., of number of rigid body elements. In the numerical experiment the force ranges up to 10^7 N and deformations up to 50% for rubber, nylon and steel.

For the twist experiment we apply a torque on the ends of the cable. The theoretical relation between twist angle and torque is $\tau = c_t\Omega = (YI_A/2(1+\sigma)L)\Omega$. The result of the twist experiment

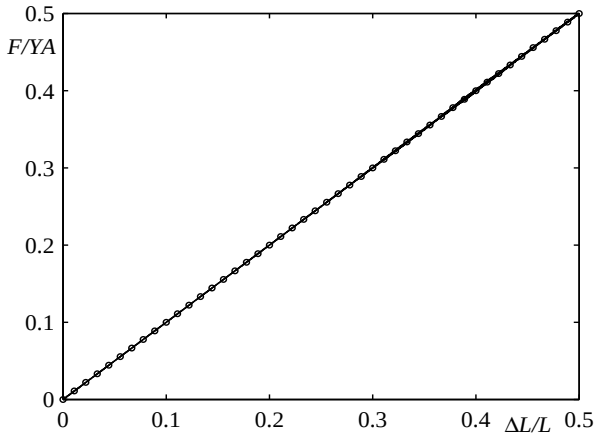

Fig. 10. Results from stretching experiments for the given set of spatial discretizations and materials. The theoretical curve is given by the solid line.

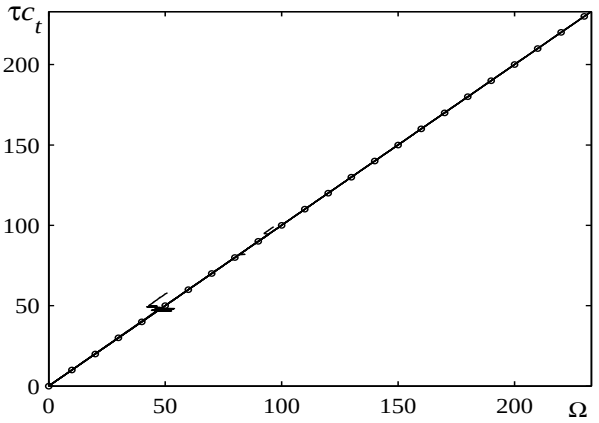

Fig. 11. Results from twisting experiments for the given set of spatial discretizations and materials. The theoretical curve is given by the solid line. The simulation develops instabilities in the regime of extreme deformations producing to large tensions, e.g., at 2.4 turns of the 10 m steel cable.

is displayed in Fig. 11. The total twist angle of the cable ranges up to 233 radians, or approximately 37 turns, except for the steel material. In the case of steel cable, the simulation becomes unstable at large tension, $\tau = 6.8\cdot 10^6$ Nm, and large rotations, 15 radians or 2.4 turns and for division with 24 segments due to spurious oscillations. The stable region for steel ranges to higher values for coarser segmentation, e.g., for division with 12 segments it ranges up to $\tau = 4.2\cdot 10^7$ Nm and 96 radians rotation , or 15 turns. However, these large tensions do not occur in reality as an actual steel cable breaks or plasticizes under such strains. Note that when the individual twist angle between two segments exceeds 2π the winding number must be included in (22) for these experiments to be possible.

The bend test is performed by applying a bending torque on the ends of the cable. The applied torque makes the cable form a circular arc with a well-defined curvature radius, see Fig. 9, that is estimated from the segments center of mass positions. The relation between torque and curvature radius from the numerical experiment is compared to the theoretical relation $\tau = YI_A/R$. The result is displayed Fig.12, with torque normalized by $\tau_1 = YI_A/1$. Except for the most coarse discretization, with $N_C = 3$, the curves

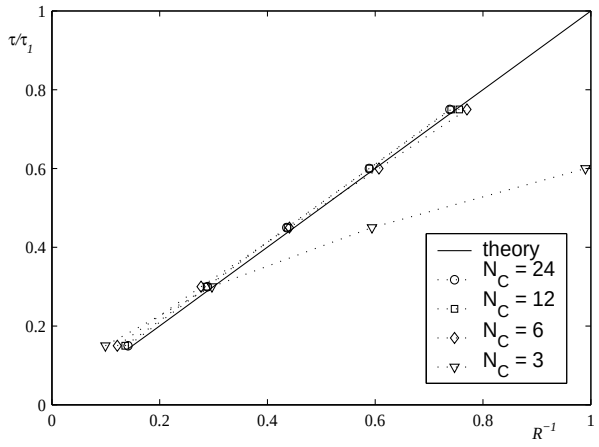

Fig. 12. Results from bending experiments for the given set of spatial discretizations. The theoretical curve is given by the solid line. Torque is normalized by normalized by $\tau_1 = YI_A/1$. For the case of discretization of the cable into three segments the error is considerable, but otherwise the values are in close agreement with theory.

fit the theory well, and increasingly so with increasing number of segments, from 10 % ($N_C = 6$) to 2.5 % ($N_C = 24$) deviation.

B. Numerical stability

Numerical stability is investigated by simulating the motion of a light cable supporting a heavy mass. One end segment of the cable is anchored to the world by a spherical constraint, and the other, heavy segment, is let to fall under gravity. The end segments are given the mass $\mathscr{M}$, whereas all other segments are of mass m. The cable is modeled using the regularized angular constraint of § V-A. Constraint forces are computed via the Schur complement method of (11). Stability is tested by giving the system a large disturbance—moving the anchor position. This induces pendulum motion with large amplitude. Instability is identified as large amplitude oscillations of the light segments. The dependency between mass ratio, cable stiffness (the Young's modulus Y and cross-section parameter β) and numerical stability is displayed in Table II. The parameter β is defined as $\beta \equiv c_s/c_b = A/I_A$ and depends on the cross-section area and shape of the cable (for a quadratic cross section $\beta = 12/A$). Outside this regime, larger mass ratios or smaller bending resistance (controlled by β), the system becomes numerically unstable and the simulation breaks down. The numbers in Table II were obtained using the alternative definition of the twist angle in § V-A. With the ordinary definition, the maximum mass ratio is a factor 10 smaller. The maximum mass ratio increases with the bending and twist elasticity. In the numerical experiments, we use the time step $\Delta t = 1/60$ s and gravity is set to $g = 10$ m/s^2. Stable simulation with mass ratios up to $\mathscr{M}/m = 10^5$ are achieved for 20 Gauss-Seidel iterations. The required number of iterations depends foremost on the mass ratio and stays relatively constant during simulation of a hoisting system. Moderate mass ratios up to $\mathscr{M}/m = 10^3$ are stable using only 3 iterations. Using the iterative solver for large mass ratios with too few iterations results in a large error, e.g., large separation between the top two elements. In a MATLAB implementation of the system, however, we achieve mass ratios of $\mathscr{M}/m = 10^9$ for the given time step $\Delta t = 1/60$ using a *direct solver* for the entire system. The conclusion is that the limit $\mathscr{M}/m = 10^5$ ($\mathscr{M}/m = 10^3$ for three iterations) can be increased considerably further by using a direct solver or an iterative solver with better convergence, e.g., a conjugate gradient solver.

TABLE II
THE MAXIMAL STABLE MASS RATIO $\mathscr{M}/m$ AND ITS DEPENDENCE ON YOUNG'S MODULUS AND CROSS-SECTION PARAMETER β.

Y (GN/M^2)	β (m^{-2})	N_C	$(\mathscr{M}/m)_{max}$
200	10^7	24	10
200	10^6	24	10^2
200	10^4	24	10^3
200	10^2	24	10^4
2000	10	24	10^5
200	...	6	10
200	...	6	10^2
200	10^3	6	10^3
200	10^2	6	10^4
2000	10	6	10^5

C. Computational performance

The computational cost of cable simulation using the methods presented in this paper is now investigated. The hardware used in these experiments consists of a Intel Pentium M 1.7 GHz processor and 512 MB RAM. Timing results are shown in Fig. 13, for 3 iterations, which by observations is enough to give stability for a cable attached to the world and supporting a heavy load so $\mathscr{M}/m = 100$. The figure shows the time spent for computing the constraint forces and the time for some of the subprocesses in doing that, namely, building the Schur complement blocks, solving the diagonal matrix equation for the first step in the Gauss-Seidel iterations (the preconditioning step) and the time for the iterations. Observe that the computational cost scales roughly linearly with the number of cable elements. This holds for longer chains as well. Thus, spending $1/60$ s on cable computations per time step, with this particular hardware, enables real-time simulation of cables with more than 100 segments. The iterations give minor contribution to the computational time and the same performance is achieved for mass ratios $\mathscr{M}/m = 10^5$ with 20 iterations and 50 elements. This number can be increased further by using faster hardware and further code optimization. By applying adaptive resolution it is possible to keep the number of elements at a minimum and increasing the resolution only locally when required. The drawback of adaptive resolution is that the computational time required at each time step varies unpredictably.

D. Limitations of the approach

In this paper we use a simple impulse based collision model with Coulomb friction. This approach can be used for handling contact between the load and other heavy or static objects and slacking cable with self-contact or contact with environment. The method presented here scales linearly with the number of cable segments. But when the cable is under large tension a more refined and robust method is needed. This is likely to introduce a dependency on the number of contacts. Preliminary investigation suggests that none of the standard techniques for rigid body contact is suitable for handling frictional contact in real-time with stable

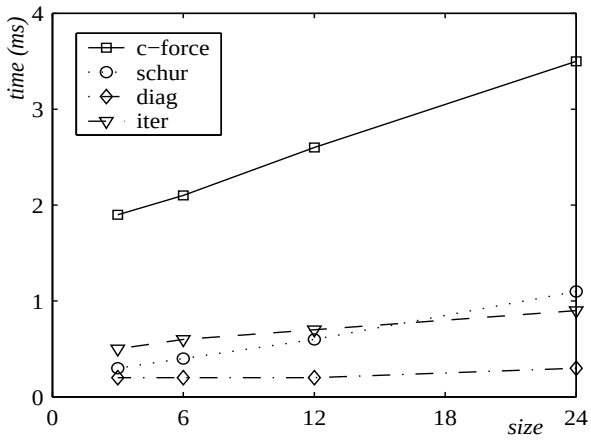

Fig. 13. Timing results with 3 iterations. 'c-force' is the total time for computing the constraint force and scales linearly with system size. The computation of the Schur complement matrix has the worst scaling.

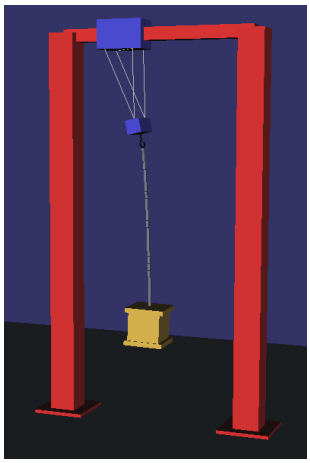

Fig. 14. A demonstration system representing a gantry crane.

result. The fact that the cable elements have very thin geometry complicates the contact issue further. This issue is the focus for future investigations. For the application context here, there is minimal contact interaction with the environment.

We have found that cable elasticity introduced as a regularized constraint improves the numerical stability and enables hoisting simulation with large mass ratios. For large mass ratios, however, the required elasticity may be stiffer than for the actual cable material. A solution to this is to make the elasticity depend on the current load force such that the cable is stabilized by an artificially large stiffness when it is under very large tension and relaxes to normal material stiffness when the load force drops, e.g., when the load is resting, allowing the cable to slack. Likeways, it should be possible to avoid unwanted bending resistance when the cable has a few contacts by reducing the stiffness at the active link. Most of the high-frequency modes in the cable will still be suppressed by the bending resistance in the other links.

The presented method is associated with numerical dissipation of the cable *deformation*. The effect on the swinging motion of hoisting systems is marginal. The nature of this dissipation and how it compares to other numerical integrators is discussed in more detail in Ref. [30].

VIII. Application to virtual environments

A visual interactive real-time simulation was built as a prototype application for testing the developed method. The package *Colosseum3D* [6], an authoring framework for VEs, was used for the graphics framework, and this was supplemented with an implementation of the rigid body cable model developed in § V and numerical integration according to Algorithm 1.

A gantry crane model was built as shown in Fig. 14, and composed as follows. A *static crane construction* (red), and a *trolley* (blue), attached to the crane beam by a lock constraint. The user interactively controls the trolley position along the beam. The trolley mass is M_{trolley}; *hook* (blue and black)—a heavy block with a hook, all modeled as a single rigid body with box geometry and mass M_{hook}; *massless cable* (light gray)—two massless cables [29], with stiffness coefficient c_{m}, runs in parallel from trolley and through the hook block and back to trolley such that the hook is suspended to slide freely along the massless cables. The free sliding represents frictionless wheels on the hook-block over which the cable may run. The user may interactively vary the length of the massless cables, pairwise correlated or individually, and thereby raise, lower or tilt the hook; *load* (yellow)—a heavy block of mass M_{load}; *rigid body cable* (gray)—rigid blocks of mass $M_{(i)}$ all connected pairwise using the angular constraint with parameters c_s, c_b, c_t. The heavy hook and load are included as the top and bottom elements of the cable, as this drastically increases the stability. The mass of the intermediate cable elements is M_{cable}.

Gravity is set to $G = 10\ m/s^2$. The system is integrated with time step $\Delta t = 1/60\ s$ using the preconditioned block Gauss-Seidel solver of § VI with 3 iterations and 10 collision iterations. The cable parameters are $c_{\text{m}} = 10^7\ N/m, c_s = 5 \cdot 10^6\ N/m, c_b = 10^3\ N/rad, c_t = 10^3\ N/rad$ and mass ratio $M_{\text{load}}/M_{\text{cable}} = 300/0.3 = 1000$. For the prototype implementation of the full crane system however, we have not achieved similar mass ratio stability as reported in § VII-B. In order to reach mass ratios of $M_{\text{load}}/M_{\text{cable}} = 10^4$, the system was stabilized by rescaling the inertia tensor of the cable elements by a factor 20. Fig. 14 shows a snapshot of the simulation. When the load rests on the ground the cable slacks, as displayed in Fig. 15, the geometrical shape of the cable depends on the material elasticity parameters.

Figure 16 displays how the energy evolves as a function of time for the crane model system with steel cable and set to swinging motion initially. The total energy drops by 20% during these 15 s and most of this during the initial 5 s. The energy loss is due to numerical dissipation of the cable *deformation* and has marginal effect on the swinging motion of the load. The nature of this dissipation and how it compares to other numerical integrators is discussed in more detail in Ref. [30].

IX. Summary and conclusions

We have found that simulating hoisting cable for VEs as rigid body elements connected by regularized constraints enables *i)* stable simulation at large mass ratios and large time steps and *ii)* physics based modeling of deformation forces with simulation parameters in direct relation to conventional material parameters.

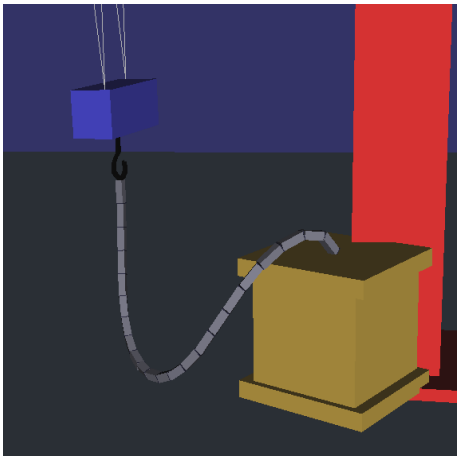

Fig. 15. The load is resting on the ground. The geometrical shape of the slacking cable depends on the elasticity of the material.

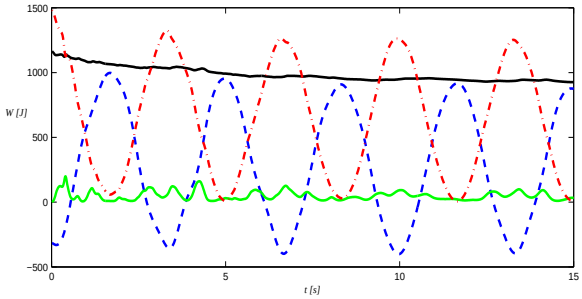

Fig. 16. Energy as a function of time for the crane model system with large swinging motion. The solid solid black line is the total energy. The other energies are the kinetic energy (red dash-dotted line), the gravitational potential energy (blue dashed line) and the cable deformation energy (green solid line).

The key is the *angular constraint*, introduced in § V, that is natural for handling deformation energies based on elasticity theory. The model can handle large deformations, e.g., twist angles exceeding 2π. We were led to this model from numerical experiments with a particle based cable model that showed that the inclusion of bending resistance to the system, as a regularized constraint, suppresses transverse high frequency oscillations and thereby increases the numerical stability. In numerical experiments with particle based cable we achieve numerically stable simulation of hoisting with mass ratios well above practical use, e.g., with load mass 10^{15} more massive than cable particles, at large time steps $\Delta t = 1/60$ *s* using symplectic-implicit mixed integration strategy. This stabilizing effect cannot be achieved using explicit bending forces. We demonstrate that efficient time integration of systems including the rigid body based cable model can be achieved. This is exemplified with an implementation where the constraint forces are computed using a block Gauss-Seidel algorithm that utilizes the sparse banded structure of the cable subsystem. In numerical experiments we demonstrate validity of the model in comparison to theoretical relations between geometrical deformation and force. Alternative measures for the bending and torsion can be found in Refs. [13] and [31] – these could also form the basis for angular constraints and deformation energy. An important choice of ours is that the torsion is computed as the angle between body fixed vectors instead of using the binormals to the curve, which tends to produce fluctuating torsional forces for an almost straight cable. The numerical stability is investigated and we find that the stability regime ranges up to mass ratios $\mathscr{M}/m = 10^5$ at time steps $\Delta t = 1/60$ s. Timing analysis show linear complexity in system size and that cables with 50–100 elements can be simulated in real-time ($\Delta t = 1/60$ s) with a hardware with modest computational speed.

The developed method meets the requirements for simulation of hoisting cable in VEs, listed in § I-A. Further experimentation and development should be done to further increase the robustness and interactivity. The experiments shows numerical instabilities when the cable is under large tensions and influenced by continuous and colliding contact. And for the simulation of the entire crane system in § VIII, we were forced to stabilize the system by rescaling the inertia tensor of the cable elements by a factor 20 in order to reach mass ratios of $M_{\text{load}}/M_{\text{cable}} = 10^4$. This defiance is, presumably, resolved by employing a less brute impulse solver or by treating contacts as a linear complementarity problem. In a MATLAB implementation of the system, however, we achieve mass ratios of $\mathscr{M}/m = 10^9$ for the given time step $\Delta t = 1/60$ using a *direct solver* for the entire system. It seems possible to significantly improve the robustness of the current system by using a direct solver or an iterative solver that converges more quickly, e.g., a conjugate gradient solver. We will consider this in future publications.

ACKNOWLEDGMENTS

The research was supported in part by ProcessIT Innovations, ”Objective 1 Norra Norrlands” EU grant awarded to HPC2N/VRlab at Umeå University and by the Swedish Foundation for Strategic Research (SSF-A3 02:128).

Many thanks to A. Backman, K. Bodin and K. Wiklund for support in development of prototype software and discussions on physical modeling for virtual environments.

REFERENCES

[1] ABDEL-RAHMAN, E. M., NAYFEH, A. H., AND MASOUD, Z. N. 2003. Dynamics and control of cranes: A review. *Journal of Vibration and Control 9*, 7, 863–908.

[2] ANTMAN, S. 2005. *Nonlinear Problems of Elasticity (Applied Mathematical Sciences)*. Springer.

[3] ASCHER, U., AND LIN, P. 1996. Sequential regularization methods for higher index DAEs with constraint singularities: The linear index-2 case. *SIAM J. Numer. Anal. 33*, 1921–1940.

[4] ASCHER, U., AND LIN, P. 1997. Sequential regularization methods for nonlinear higher index DAEs. *SIAM J. Scient. Comput 18*, 160–181.

[5] ASCHER, U., CHIN, H., PETZOLD, L., AND REICH, S. 1995. Stabilization of constrained mechanical systems with DAEs and invariant manifolds. *Mech. Struct. & Mach. 23*, 135–158.

[6] BACKMAN, A. 2005. Colosseum3D - authoring framework for virtual environments. In *Proceedings of 11th EGVE Workshop*, Eurographics Association, Aalborg University, Denmark, 225–226.

[7] BANERJEE, A. K., AND NAGARAJAN, S. 1997. Efficient simulation of large overall motion of beams undergoing large deflection. *Multibody System Dynamics 1*, 1, 113–126.

[8] BARAFF, D. 1996. Linear-time dynamics using Lagrange multipliers. *Computer Graphics 30*, Annual Conference Series, 137–146.

[9] BAUMGARTE, J. 1972. Stabilization of constraints and integrals of motion in dynamical systems. *Computer Methods in Applied Mechanics and Engineering 1*, 1, 1–16.

[10] BRAESS, D. 1997. *Finite Elements: Theory, Fast Solvers, and Applications in Solid Mechanics*. Cambridge University Press, Cambridge, U. K.

[11] ERLEBEN, K., SPORRING, J., HENRIKSEN, K., AND DOHLMANN, H. 2005. *Physics-based Animation*. Charles River Media.

[12] FEATHERSTONE, R. 1999. *Divide-and-Conquer Articulated-Body Algorithm for Parallel O(log(n)) Calculation of Rigid-Body Dynamics" Part 1: Basic Algorithm.. Int. J. Robotics Research*, vol. 18, no. 9, pp. 867–875.

[13] GREGOIRE, M., AND SCHÖMER, E. 2007. *Interactive simulation of one-dimensional flexible parts.. Computer-Aided Design*, 39 (8), pp. 694–707.

[14] HAIRER, E., LUBICH, C., AND WANNER, G. 2001. *Geometric Numerical Integration*, vol. 31 of *Spring Series in Computational Mathematics*. Springer-Verlag, Berlin, Heidelberg, New York, London, Paris, Tokyo, Hong Kong.

[15] HEYDEN, T., AND WOERNLE, C. 2006. Dynamics and flatness-based control of a kinematically undetermined cable suspension manipulator. *Multibody System Dynamics 16*, 2, 155–177.

[16] KAMMAN, J., AND HUSTON, R. 2001. Multibody dynamics modeling of variable length cable system. *Multibody System Dynamics 5*, 3, 211–221.

[17] KANG, S.-C., AND MIRANDA, E. 2004. Physics based model for simulating the dynamics of tower cranes. *International Conference on Computing in Civil and Building Engineering, ICCCBE, Weimar, Bauhaus-Universität, Germany 10*, 248–253.

[18] KHAREVYCH, L., WEIWEI, TONG, Y., KANSO, E., MARSDEN, J. E., SCHRÖDER, P., AND DESBRUN, M. 2006. Geometric, variational integrators for computer animation. *SCA '06: Proceedings of the 2006 ACM SIGGRAPH/Eurographics symposium on Computer animation, Vienna, Austria*, 43–51.

[19] KISS, B., LÉVINE, J., AND MÜLLHAUPT, P. 1999. Modelling, flatness and simulation of a class of cranes. *Periodica Polytechnica Electrical Engineering, 43*, 03, 215–225.

[20] LACOURSIÈRE, C. 2006. A regularized time stepper for multibody systems. Tech. Rep. UMINF 06.04 ISSN-0348-0542, Dept. of Computing Science, Umeå University, Mar.

[21] LACOURSIÈRE, C. 2007. *Ghosts and Machines: Regularized Variational Methods for Interactive Simulations of Multibodies with Dry Frictional Contacts*. PhD thesis, Department of Computing Science, Umeå University, Sweden, SE-901 87, Umeå, Sweden.

[22] LANDAU, L., AND LIFSCHITZ, E. 1986. *Theory of Elasticity*. Pergamon Press, Oxford, 3rd ed.

[23] LOOCK, A., AND SCHÖMER, E. 2001. A virtual environment for interactive assembly simulation: From rigid bodies to deformable cables. In *5th World Multiconference on Systemics, Cybernetics and Informatics (SCI'01), Vol. 3 (Virtual Engineering and Emergent Computing)*, 325–332.

[24] MULLER, M., HEIDELBERGER, B., TESCHNER, M., AND GROSS, M. 2005. Meshless deformations based on shape matching. *ACM TRANSACTIONS ON GRAPHICS 24* (July), 471–478.

[25] OH, S., AHN, J., AND WO, K. 2006. Low damped cloth simulation. *Visual Comput. 22*, 2 (Feb.), 70–79.

[26] PAI, K. 2002. STRANDS: Interactive simulation of thin solids using cosserat models. *Computer Graphics Forum 21*, 3, 347–352.

[27] REDON, S., GALOPPO, N., AND LIN, M. C. 2005. Adaptive dynamics of articulated bodies. *ACM Transactions on Graphics 24*, 3 (July), 936–945.

[28] RÉMION, Y., NOURRIT, J.-M., AND GILLARD, D. 1999. Dynamic animation of spline like objects. In *WSCG'99 Conference Proceedings*, V. Skala, Ed., 426–432.

[29] SERVIN, M., LACOURSIÈRE C. 2007. Massless cable for real-time simulation. *Computer Graphics Forum 26*, 2 (June), 172–184.

[30] SERVIN, M., LACOURSIÈRE, C., AND MELIN, N. 2006. Interactive simulation of elastic deformable materials. In *Proceedings of SIGRAD Conference 2006 in Skövde, Sweden*, Linköping University Electronic Press, Linköping, 22–32.

[31] SPILLMANN, J., AND TESCHNER, M. 2007. CORDE: Cosserat Rod Elements for the Dynamic Simulation of One-Dimensional Elastic Objects. In *Proc. ACM SIGGRAPH / Eurographics Symposium on Computer Animation*, San Diego, USA, pp. 209–217.

[32] TESCHNER, M., HEIDELBERGER, B., MULLER, M., AND GROSS, M. 2004. A versatile and robust model for geometrically complex deformable solids. *COMPUTER GRAPHICS INTERNATIONAL, PROCEEDINGS*, 312–319.

[33] UMFPACK `http://www.cise.ufl.edu/research/sparse/umfpack/`

[34] WEINSTEIN, R., TERAN, J. AND FEDKIW, R. 2006. *Dynamic Simulation of Articulated Rigid Bodies with Contact and Collision. IEEE TVCG*, 12, pp 365–374.

[35] VON SCHWERIN, R. 1999. *Multibody System Simulation; Numerical Methods, Algorithms, and Software*. Springer Verlag, Berlin.

Martin Servin Martin Servin is lecturer at the department of Physics at Umeå University. He received his MSc and PhD degrees in theoretical physics from Umeå University in 1999 and 2003, respectively. His research interests include physical modeling and simulation for real-time interactive 3D graphics. He is director for the research center IFOR (Intelligent Vehicles Off-Road).

Claude Lacoursière Claude Lacoursière is a research assistant at the department of Computing Science at Umeå University. He completed his MSc at the physics department of McGill University in 1993 and his PhD at Umeå University in 2007. In the meantime, he worked at physics simulations companies based in Montréal. His research interests include physics motivated numerical methods for real-time integration of mechanical systems, especially contacting multibodies subject to dry friction.